

Theoretical study of the electronic states of hollandite vanadate $\text{K}_2\text{V}_8\text{O}_{16}$

S. Horiuchi, T. Shirakawa, and Y. Ohta

Department of Physics, Chiba University, Inage-ku, Chiba 263-8522, Japan

(Dated: 20 December 2007)

We consider electronic properties of hollandite vanadate $\text{K}_2\text{V}_8\text{O}_{16}$, a one-dimensional zigzag-chain system of t_{2g} orbitals in a mixed valent state. We first calculate the Madelung energy and obtain the relative stability of several charge-ordering patterns to determine the most stable one that is consistent with the observed superlattice structure. We then develop the strong-coupling perturbation theory to derive the effective spin-orbit Hamiltonian, starting from the triply-degenerate t_{2g} orbitals in the VO_6 octahedral structure. We apply an exact-diagonalization technique on small clusters of this Hamiltonian and obtain the orbital-ordering pattern and spin structures in the ground state. We thereby discuss the electronic and magnetic properties of $\text{K}_2\text{V}_8\text{O}_{16}$ including predictions on the outcome of future experimental studies.

PACS numbers: 71.10.-w, 71.30.+h, 75.10.-b, 71.20.Be

I. INTRODUCTION

In the study of strongly correlated electron systems, vanadium oxide has been one of the central materials. In particular, the discovery of the phase transition associated with the reduction of the magnetic susceptibility in a mixed valence compound $\alpha'\text{-NaV}_2\text{O}_5$,^{1,2} together with subsequent experimental and theoretical studies, has established the novel concept of the charge-ordering (CO) phase transition accompanied by the spin-singlet formation.

Recently, Isobe *et al.*³ reported that, in hollandite vanadate $\text{K}_2\text{V}_8\text{O}_{16}$, a metal-insulator transition (MIT) occurs at ~ 170 K, which is accompanied by the rapid reduction of the magnetic susceptibility. Below the transition temperature, a characteristic superlattice of $\sqrt{2}a \times \sqrt{2}a \times 2c$ is observed,³ whereby a possible CO phase transition accompanied by the spin-singlet formation was proposed.³

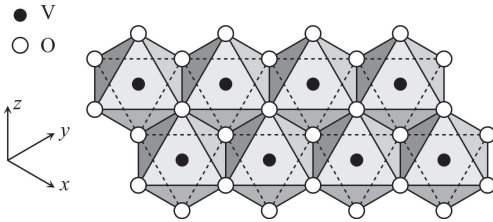


FIG. 1: Schematic representation of the double string of edge-shared VO_6 octahedra in $\text{K}_2\text{V}_8\text{O}_{16}$.

The crystal structure of this compound belongs to a group of hollandite-type phases and has a V_8O_{16} framework composed of double strings of edge-shared VO_6 octahedra as shown in Fig. 1. In the view of orbital physics, this system may be regarded as a one-dimensional (1D) version of LiVO_2 known as a possible orbital-ordering (OO) system of the t_{2g} orbitals on the 2D triangular lattice of $S = 1$ spins,^{4,5} as in the case of a similar hollandite vanadate $\text{Bi}_x\text{V}_8\text{O}_{16}$.^{6,7} The present system $\text{K}_2\text{V}_8\text{O}_{16}$

however has the average valence of $\text{V}^{3.75+}$ and thus is in the mixed valent state of $\text{V}^{3+} : \text{V}^{4+} = 3d^2 : 3d^1 = 1 : 3$, for which quite different electronic states are expected. Thus, the central issue in the present system is the mechanism of the MIT concerning how the highly frustrated spin, charge, and orbital degrees of freedom at high temperatures are relaxed by lowering temperatures and what type of orders is realized in the ground state.

In this paper, we first examine the charge degrees of freedom of this system by calculating the Madelung energy; we obtain several CO patterns and their relative stability to determine the most stable one that is consistent with the characteristic superlattice structure observed in the low-temperature phase of the material. We then develop the strong-coupling perturbation theory starting from the triply-degenerate t_{2g} orbitals in the VO_6 octahedral structure and derive the effective spin-orbit Hamiltonian in the approximation of neglecting the orbital fluctuations. We apply an exact-diagonalization technique on small clusters to this Hamiltonian and obtain the OO pattern and spin-spin correlation functions in the ground state. We thereby suggest that the state of local singlets of two $s = 1/2$ spins coexisting with local high-spin clusters of $S = 3/2$ should be of possible relevance with the observed electronic and magnetic states of $\text{K}_2\text{V}_8\text{O}_{16}$.

This paper is organized as follows: In Sec. II, we calculate the CO pattern within the ionic model and derive the effective spin-orbit Hamiltonian based on the perturbation theory. In Sec. III, we calculate the orbital and spin structures of the derived effective Hamiltonian and compare the results with experiment. Summary is given in Sec. IV.

II. EFFECTIVE HAMILTONIAN

Here, we derive the effective spin-orbit Hamiltonian based on the strong-coupling perturbation theory, where the unperturbed state adopted is the lowest-energy CO state obtained from the ionic model in the limit of van-

ishing hopping parameters.

A. Madelung energy and CO patterns

To determine the CO pattern in the ground state of $\text{K}_2\text{V}_8\text{O}_{16}$, we adopt the ionic model and calculate the Madelung energy,⁸ the electrostatic energy of an assembly of positive and negative point charges of the ions, which is known to be a good measure for the relative stability of the spatial distributions of d electrons in transition-metal oxides^{9,10} as well as the CO patterns of some organic charge-transfer salts.¹¹ We assume various d electron distributions on the V ions and compare the Madelung energies where we use the room-temperature crystal structure reported for $\text{K}_2\text{V}_8\text{O}_{16}$.¹² We first calculate the Madelung energy for the system with a hypothetical uniform electron distribution, where all the V ions are assumed to have the valence state of $\text{V}^{3.75+}$; we find the energy of -3341.386 eV/sc where sc is the unit cell of the observed $\sqrt{2}a \times \sqrt{2}a \times 2c$ superlattice. We then calculate the Madelung energies for various CO patterns with V^{3+} or V^{4+} and find that a number of CO patterns are more stable than the energy for the uniform electron distribution. The most stable CO pattern that is consistent with the superlattice structure observed in the low-temperature phase of this material is found to have the energy of -3370.546 eV/sc. We point out that the obtained low-energy CO patterns commonly have the CO state illustrated in Fig. 2; i.e., the 1D zigzag chain consisting of V ions always has this CO state. Therefore, we hereafter assume that this CO pattern is realized in $\text{K}_2\text{V}_8\text{O}_{16}$. We note that this CO pattern is different from the one proposed by Isobe *et al.* (see Fig. 4 of Ref. 3), which has a much higher Madelung energy -3327.885 eV/sc. Detailed discussions on the CO patterns are given in Ref. 13.

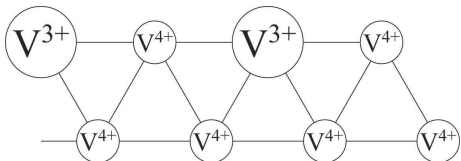


FIG. 2: Most stable CO pattern in $\text{K}_2\text{V}_8\text{O}_{16}$ obtained from the Madelung energy calculations. Only a single zigzag chain of V ions in the material is illustrated.

B. Perturbation theory

Here, we develop the strong-coupling perturbation theory starting from the ground state in the strong-coupling limit, i.e., the CO state shown in Fig. 2. Our starting

high-energy Hamiltonian is of the following form:

$$H = H_0 + H_t \quad (1)$$

$$H_0 = V \sum_{\langle ij \rangle} n_i n_j + V' \sum_{[ij]} n_i n_j - J_H \sum_{i\sigma\sigma', \alpha\neq\beta} c_{i\alpha\sigma}^\dagger c_{i\beta\sigma'}^\dagger c_{i\beta\sigma} c_{i\alpha\sigma'} + U \sum_{i\alpha} n_{i\alpha\uparrow} n_{i\alpha\downarrow} + U' \sum_{i, \alpha\neq\beta} n_{i\alpha} n_{i\beta} \quad (2)$$

$$H_t = - \sum_{\langle i\alpha, j\beta \rangle, \sigma} t_{i\alpha, j\beta} (c_{i\alpha\sigma}^\dagger c_{j\beta\sigma} + \text{H.c.}) \quad (3)$$

where $c_{i\alpha\sigma}^\dagger$ ($c_{i\alpha\sigma}$) is the creation (annihilation) operator of an electron at site i , orbital α , and spin $\sigma = \uparrow, \downarrow$. We define the number operators $n_{i\alpha\sigma} = c_{i\alpha\sigma}^\dagger c_{i\alpha\sigma}$, $n_{i\alpha} = n_{i\alpha\uparrow} + n_{i\alpha\downarrow}$, and $n_i = \sum_{\alpha} n_{i\alpha}$. V and V' are the intersite Coulomb repulsions between nearest-neighbor and next-nearest-neighbor sites, respectively. J_H is the Hund's rule coupling, and U and U' are the intra- and inter-orbital on-site Coulomb repulsions, respectively. We assume the relation $U' = U - 2J_H$ throughout the paper, which is valid in the atomic limit. $t_{i\alpha, j\beta}$ is the hopping parameter between the orbital α on site i and orbital β on site j where $\alpha, \beta \in \{d_{xy}, d_{yz}, d_{zx}\}$ in the coordinate system shown in Fig. 1. We retain only the direct V-V hoppings between the t_{2g} orbitals because the indirect hoppings via the O ions are rather small.⁴ We then have the independent nearest-neighbor hopping parameters t_a , t_b , and t_c as shown in Fig. 3.

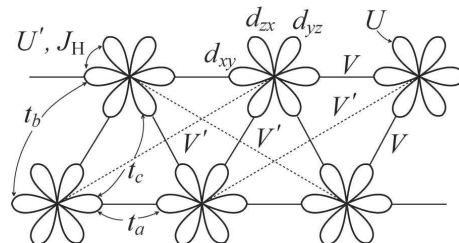


FIG. 3: Schematic representation of the t_{2g} orbitals on the 1D zigzag chain of $\text{K}_2\text{V}_8\text{O}_{16}$. Two of the four lobes for each of the three t_{2g} orbitals are drawn.

We assume that the ground state of our Hamiltonian H_0 should have the CO pattern shown in Fig. 2, where there are no doubly occupied orbitals and no V^{2+} or V^{5+} ionic states since these states are highly unrealistic in this material. We therefore impose the condition

$$U' - 2V - J_H > 0. \quad (4)$$

We should also note that the unperturbed ($H_t = 0$) states are spin- and orbital-degenerate of the degeneracy $M = 3^N \cdot 3^{N/4} \cdot 2^{3N/4}$ where N is the number of sites. This degeneracy is lifted by the perturbation processes. We develop the second-order perturbation calculation with

respect to $t_{i\alpha,j\beta}$ assuming that $t_{i\alpha,j\beta}$ is much smaller than $U, U', V,$ and V' . We thereby derive the effective spin-orbit Hamiltonian:

$$H_{\text{eff}} = H_0 - \sum_{\mu\mu'} |\mu\rangle \sum_n \frac{\langle\mu|H_t|n\rangle\langle n|H_t|\mu'\rangle}{E_n - E_0} \langle\mu'| \quad (5)$$

where $|\mu\rangle$ and $|\mu'\rangle$ ($\mu, \mu' = 1, \dots, M$) are the M independent eigenvectors of the ground state of H_0 and $|n\rangle$ is the n -th excited state of H_0 . E_n is the corresponding eigenenergy of H_0 ($n = 0$ denotes the ground state).

To consider the real material, we should take into account the effect of distortion of the VO_6 octahedra more carefully because the degeneracy of the t_{2g} orbitals can be lifted. To evaluate the effect of distortion, we calculate the local symmetry of the Madelung site potential ϕ in the point charge model for the real material. Calculated result shows that the orbital d_{xy} (see Fig. 3) is much less stable for the electron to sit on than the other orbitals d_{yz} and d_{zx} are; i.e. $\phi_{xy} > \phi_{yz} = \phi_{zx}$, where we also point out that the two orbitals d_{yz} and d_{zx} are exactly degenerate due to symmetry of the lattice. We therefore assume that the electrons do not occupy the d_{xy} orbital in the ground state as well as in the perturbation processes. A recent NMR experiment¹⁴ seems to support this assumption.

We introduce an approximation here; because the hopping parameters $t_{i\alpha,j\beta}$ take the values $t_a \gg t_b \simeq t_c$, we assume $t_b = t_c = 0$ for simplicity as in Refs. 4 and 7. This approximation means that the terms like $H_{ij}^{\text{eff}} \propto t_a t_c$ and $H_{ij}^{\text{eff}} \propto t_b t_c$ are all neglected, retaining only the terms like $H_{ij}^{\text{eff}} \propto t_a^2$ in the second-order processes. Note that the orbital fluctuations are completely suppressed in this approximation because only two orbitals connected with the *diagonal* hopping t_a come out and no *off-diagonal* hopping terms appear in the effective Hamiltonian. We then obtain the effective spin-orbit Hamiltonian consisting of orbital-diagonal spin-subblocks with vanishing orbital off-diagonal blocks.

In the obtained effective spin-orbit Hamiltonian, we have five types of the bonds with different spin exchange interactions as shown in Fig. 4; three of them (denoted as FM-1, 2, 3) are the bonds with ferromagnetic exchange interaction due to double-exchange or Hund's rule coupling mechanisms and two of them (denoted as AF-1, 2) are the bonds with antiferromagnetic exchange interaction due to kinetic-exchange mechanism. Defining the spin-1 operator on site i as \mathbf{S}_i and spin-1/2 operator on site i as \mathbf{s}_i , we have the following Hamiltonian for each bond shown in Fig. 4.

(a) The bond FM-1 obtained with the process $d_i^2 d_j^1 \rightarrow d_i^1 d_j^2 \rightarrow d_i^2 d_j^1$:

$$\begin{aligned} H_{ij}^{\text{eff}} &= -2J \mathbf{S}_i \cdot \mathbf{s}_j + c \hat{1} \\ J &= \frac{t_a^2}{4V'} - \frac{t_a^2}{4(V' + 2J_{\text{H}})} \\ c &= -\frac{3t_a^2}{4V'} - \frac{t_a^2}{4(V' + 2J_{\text{H}})}. \end{aligned} \quad (6)$$

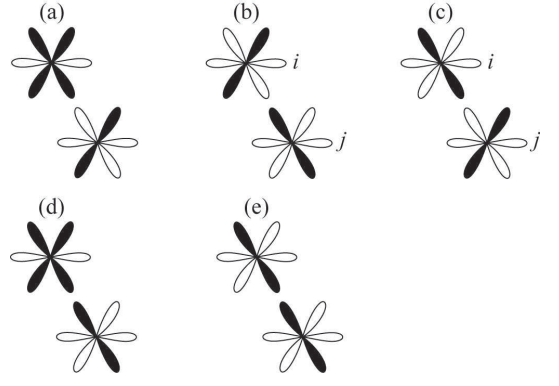


FIG. 4: Schematic representation of five types of the bonds with different exchange interaction. Electrons are located in the shaded lobes. (a) FM-1: the ferromagnetic bond with the process $d_i^2 d_j^1 \rightarrow d_i^1 d_j^2 \rightarrow d_i^2 d_j^1$, (b) FM-2: the ferromagnetic bond with the process $d_i^1 d_j^1 \rightarrow d_i^2 d_j^0 \rightarrow d_i^1 d_j^1$, (c) FM-3: the ferromagnetic bond with the process $d_i^1 d_j^1 \rightarrow d_i^0 d_j^2 \rightarrow d_i^1 d_j^1$, (d) AF-1: the antiferromagnetic bond with the process $d_i^2 d_j^1 \rightarrow d_i^3 d_j^0$ or $d_i^1 d_j^2 \rightarrow d_i^2 d_j^1$, and (e) AF-2: the antiferromagnetic bond with the process $d_i^1 d_j^1 \rightarrow d_i^2 d_j^0$ or $d_i^0 d_j^2 \rightarrow d_i^1 d_j^1$. Here, we assume that the site i denotes the site of the upper chain of Fig. 2, i.e., $\text{V}^{3+}\text{-V}^{4+}\text{-V}^{3+}\text{-V}^{4+}$ chain, and the site j denotes the sites of the lower chain of Fig. 2, i.e., $\text{V}^{4+}\text{-V}^{4+}\text{-V}^{4+}$ chain.

(b) The bond FM-2 obtained with the process $d_i^1 d_j^1 \rightarrow d_i^2 d_j^0 \rightarrow d_i^1 d_j^1$:

$$\begin{aligned} H_{ij}^{\text{eff}} &= -4J \mathbf{s}_i \cdot \mathbf{s}_j + c \hat{1} \\ J &= \frac{t_a^2}{4(U' - V' - J_{\text{H}})} - \frac{t_a^2}{4(U' - V' + J_{\text{H}})} \\ c &= -\frac{3t_a^2}{4(U' - V' - J_{\text{H}})} - \frac{t_a^2}{4(U' - V' + J_{\text{H}})}. \end{aligned} \quad (7)$$

(c) The bond FM-3 obtained with the process $d_i^1 d_j^1 \rightarrow d_i^0 d_j^2 \rightarrow d_i^1 d_j^1$:

$$\begin{aligned} H_{ij}^{\text{eff}} &= -4J \mathbf{s}_i \cdot \mathbf{s}_j + c \hat{1} \\ J &= \frac{t_a^2}{4(U' - 2V + V' - J_{\text{H}})} - \frac{t_a^2}{4(U' - 2V + V' + J_{\text{H}})} \\ c &= -\frac{3t_a^2}{4(U' - 2V + V' - J_{\text{H}})} - \frac{t_a^2}{4(U' - 2V + V' + J_{\text{H}})}. \end{aligned} \quad (8)$$

(d) The bond AF-1 obtained with the process $d_i^2 d_j^1 \rightarrow d_i^3 d_j^0$ or $d_i^1 d_j^2 \rightarrow d_i^2 d_j^1$:

$$\begin{aligned} H_{ij}^{\text{eff}} &= 2J \mathbf{S}_i \cdot \mathbf{s}_j + c \hat{1} \\ J &= -c = \frac{t_a^2}{2(U + U' - 2V - V')} + \frac{t_a^2}{2(U - U' + V' + J_{\text{H}})}. \end{aligned} \quad (9)$$

(e) The bond AF-2 obtained with the process $d_i^1 d_j^1 \rightarrow$

$d_i^2 d_j^0$ or $d_i^0 d_j^2 \rightarrow d_i^1 d_j^1$:

$$H_{ij}^{\text{eff}} = 4J \mathbf{s}_i \cdot \mathbf{s}_j + c \hat{1} \quad (10)$$

$$J = -c = \frac{t_a^2}{2(U - V')} + \frac{t_a^2}{2(U - 2V + V')}.$$

Here, $\hat{1}$ is the unit operator and we assume that the site i denotes the site of the upper chain of Fig. 2, i.e., V^{3+} - V^{4+} - V^{3+} - V^{4+} chain, and the site j denotes the sites of the lower chain of Fig. 2, i.e., V^{4+} - V^{4+} - V^{4+} chain.

Thus, we obtain the effective spin-orbit Hamiltonian

$$H_{\text{eff}} = \sum_{\langle ij \rangle} H_{ij}^{\text{eff}} \quad (11)$$

where the sum runs over all the nearest-neighbor pairs of sites. Note that this effective spin-orbit Hamiltonian has the form of block-diagonal in the spin \otimes orbital space; i.e., orbital off-diagonal blocks are all zero. In other words, we have several OO patterns for the N -site systems, and each of them, we have the spin Hamiltonian. By diagonalizing all the spin Hamiltonians, we can obtain the eigenstates of our effective spin-orbit Hamiltonian. In particular, from the lowest-energy eigenstate obtained, we determine the OO pattern of the ground state in the parameter space.

III. RESULTS OF CALCULATION

In this section, we calculate the orbital and spin structures in the ground state of the effective spin-orbit Hamiltonian Eq. (11) by using the exact-diagonalization technique on small clusters, whereby we discuss its electronic and magnetic properties and compare them with experiment. We assume $U' = U - 2J_H$ throughout the calculations.

A. Orbital ordering

We here use the 16-site cluster with four $S = 1$ spins and twelve $s = 1/2$ spins (corresponding to the filling of 20 electrons), where the spins are coupled with the exchange interactions derived in Sec. II. The periodic boundary condition is used. Calculations are made for all possible OO patterns that are consistent with the two-fold periodicity along the c -axis observed in experiment; i.e., we assume the unit cell in the presence of the orbital ordering, which contains the 4 sites along the chain direction (e.g., sites 1 – 4 in Fig. 5 (b)). Hereafter we assume the relation $V' = 0.6V$ estimated from the experimental interatomic distances between V ions.

The calculated result is shown in Fig. 5, where we find that the unique orbital state illustrated in Fig. 5 (b) with the total-spin quantum number $S_{\text{tot}} = 0$ is realized in the entire parameter space shown in Fig. 5 (a) unless the CO state is unstable. The parameter space shown in

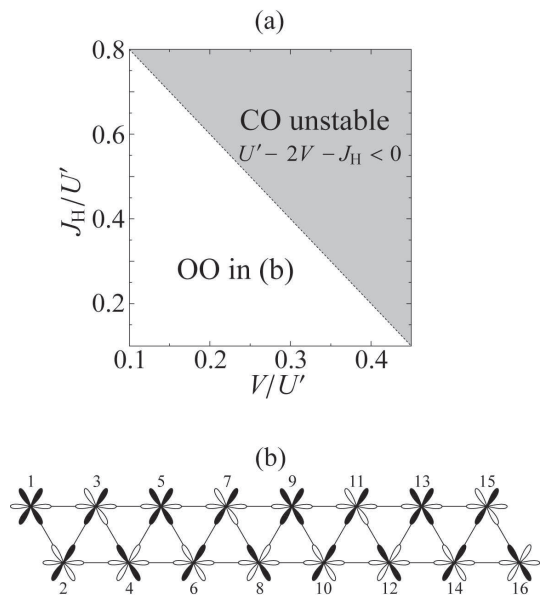


FIG. 5: (a) Ground-state phase diagram of the effective spin-orbit Hamiltonian. The CO pattern shown in Fig. 2 is unstable in the shaded region. (b) Schematic representation of the calculated OO state in the lower-left region of the upper panel (a).

Fig. 5 (a) may be presumed to contain physically realistic values for vanadium oxide materials.¹⁵ Note that this orbital state is stabilized by maximizing the number of the FM-1 bonds as shown below.

In Fig. 6, we show calculated values of the exchange coupling constant J and constant c in the effective spin-orbit Hamiltonian Eqs. (6)-(10). We find that the value of c is predominantly lower for the FM-1 bond in the entire parameter space shown in Fig. 5 (a). Thus, we understand that the OO pattern shown in Fig. 5 (b) is stabilized by maximizing the number of this FM-1 bond. We should however note that, although in the small V/U' region the value of J for the FM-1 bond is larger than those of the other bonds, the values of J for the anti-ferromagnetic bonds are much larger than those for the ferromagnetic bonds in the large V/U' region. In particular, a large value of J for the AF-2 bond in the large V/U' region is essential for the formation of the local spin-singlet of the two $s = 1/2$ spins as shown below. We thus find that the spin structure can be quite different in the different regions in Fig. 5 (a) although the unique OO pattern shown in Fig. 5 (b) is stabilized.

B. Spin correlations

We calculate the spin-spin correlation functions $\langle \mathbf{S}_i \cdot \mathbf{S}_j \rangle$, $\langle \mathbf{S}_i \cdot \mathbf{s}_j \rangle$, and $\langle \mathbf{s}_i \cdot \mathbf{s}_j \rangle$ for the ground state of the 16-site cluster of the effective spin-orbit Hamiltonian to discuss the spin structures of the system. The results are

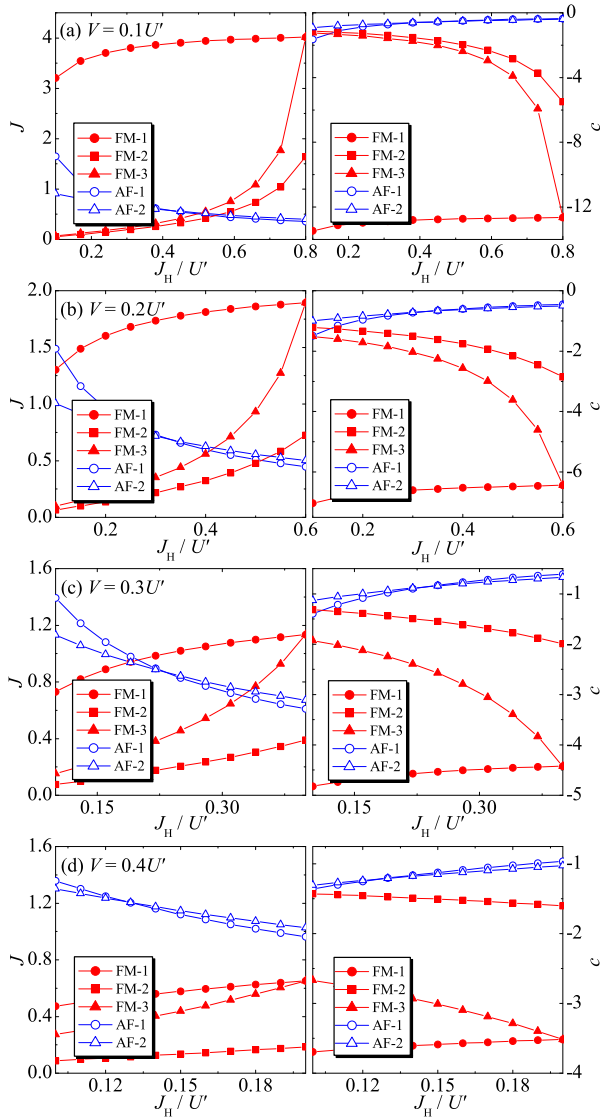


FIG. 6: (Color online) Calculated values of the exchange coupling constant J (left panels) and the constant c (right panels) given in units of t_a^2/U' .

shown in Fig. 7, where we in particular show $\langle \mathbf{S}_1 \cdot \mathbf{s}_i \rangle$ for $i \in s = 1/2$ and $\langle \mathbf{S}_1 \cdot \mathbf{S}_i \rangle/2$ for $i \in S = 1$ in the left panels of Fig. 7, and $\langle \mathbf{s}_2 \cdot \mathbf{s}_i \rangle$ for $i \in s = 1/2$ and $\langle \mathbf{s}_2 \cdot \mathbf{S}_i \rangle/2$ for $i \in S = 1$ in the right panels of Fig. 7.

We find in Fig. 7 that the behavior of the spin correlations is very different between two regions of the OO phase in the white triangle area of Fig. 5 (a): i.e., the regions $J_H \gg V$ and $V \gg J_H$. This result suggests that, although the OO pattern is the same and the total spin $S_{\text{tot}} = 0$ in the two regions, two different spin structures can be realized depending on the parameter values.

In the region $J_H \gg V$, we find the results that can roughly be described by the situation where the local high-spin clusters of $S = 5/2$ formed by four V ions are coupled antiferromagnetically; we find the values

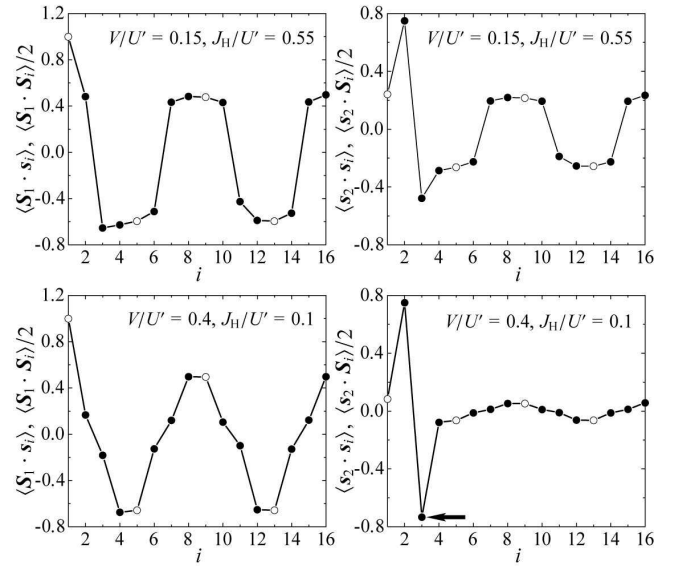


FIG. 7: Spin-spin correlation functions calculated for the ground state of the 16-site cluster. The site index i is defined in Fig. 5 (b); the symbols \circ and \bullet indicate the sites with $S = 1$ and $s = 1/2$, respectively. Left and right panels represent the spin correlations from the site 1 ($S = 1$) and site 2 ($s = 1/2$), respectively. Upper and lower panels represent the spin correlations in the parameter regions $J_H \gg V$ and $V \gg J_H$, respectively. The arrow in the lower right panel indicates the formation of the local spin-singlet of the two $s = 1/2$ spins.

$\langle \mathbf{S}_1 \cdot \mathbf{s}_2 \rangle = 0.482$, $\langle \mathbf{S}_1 \cdot \mathbf{s}_{15} \rangle = 0.435$, and $\langle \mathbf{S}_1 \cdot \mathbf{s}_{16} \rangle = 0.498$, which should be 0.5 if the formation of the high-spin cluster of $S = 5/2$ were complete. We also find the values $\langle \mathbf{s}_2 \cdot \mathbf{S}_1 \rangle/2 = 0.241$, $\langle \mathbf{s}_2 \cdot \mathbf{s}_{15} \rangle = 0.194$, and $\langle \mathbf{s}_2 \cdot \mathbf{s}_{16} \rangle = 0.234$, which should be 0.25 if the formation of the high-spin cluster of $S = 5/2$ were complete. We also find the oscillations of ± 0.5 (± 0.25) between two clusters of four spins in the upper-left (upper-right) panel of Fig. 7. Thus, our system in this parameter region can be regarded as the state of the antiferromagnetically fluctuating local high-spin clusters of $S = 5/2$. This state is illustrated schematically in Fig. 8 (a).

In the region $V \gg J_H$, we find the results that can roughly be described by the situation where the local spin-singlet states are formed between two $s = 1/2$ spins; we find the value $\langle \mathbf{s}_2 \cdot \mathbf{s}_3 \rangle = -0.734$, which is only slightly larger than the value -0.75 that is expected when the spin-singlet formation is complete. We also note that the values of $\langle \mathbf{s}_2 \cdot \mathbf{s}_i \rangle$ and $\langle \mathbf{s}_2 \cdot \mathbf{S}_i \rangle$ are very small for all i except $i = 3$, which is consistent with the formation of the local spin-singlet state. We should however find the value $\langle \mathbf{S}_1 \cdot \mathbf{s}_{16} \rangle = 0.498$, which indicates the formation of the high-spin cluster of $S = 3/2$ between the two spins at sites 1 and 16. We also note that the oscillation of ± 0.5 between clusters of the two spins appears. Thus, there remains antiferromagnetic correlations be-

tween the high-spin clusters of $S = 3/2$. This correlation occurs because the spin-singlet formation is strong but not perfect. Thus, our system in this parameter region can be regarded as the state of the local spin-singlets of two $s = 1/2$ spins coexisting with the antiferromagnetically fluctuating local high-spin clusters of $S = 3/2$. This state is illustrated schematically in Fig. 8 (b).

The spin structures thus obtained are compared with available experimental data in the next subsection.

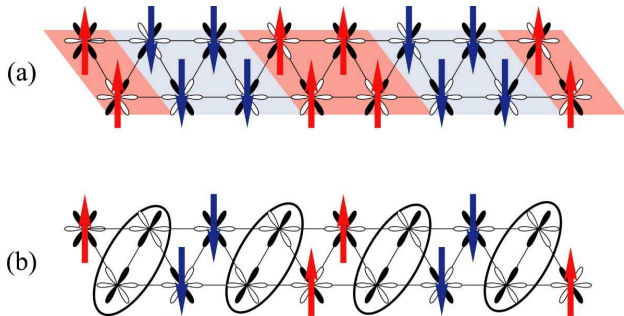


FIG. 8: (Color online) Schematic representation of the spin structures. (a) The state of the antiferromagnetically fluctuating local high-spin clusters. (b) The state of the local spin-singlets of two $s = 1/2$ spins (indicated by solid circles) coexisting with the local high-spin clusters of $S = 3/2$.

C. Comparison with experiment

In the present theory, we have presumed that the MIT observed in $\text{K}_2\text{V}_8\text{O}_{16}$ is caused by the CO of d -electrons on the V ions. We suppose this to be quite a natural interpretation because of the various features observed in experiment;³ e.g., the characteristic superlattice structure and lattice distortion observed below the transition temperature. We have also assumed that the electrons do not occupy the d_{xy} orbital (see Fig. 3) as can be justified from the calculation of the Madelung site potential. This is also consistent with the recent NMR measurement¹⁴ of the symmetry axis of this material at room temperature. These results first of all support the validity of our effective spin-orbit Hamiltonian derived in Sec. II.

Then, as for the magnetic aspects of $\text{K}_2\text{V}_8\text{O}_{16}$, the rapid reduction of the magnetic susceptibility observed below the transition temperature seems to suggest the opening of the spin gap. It seems however that a small but finite value of the susceptibility remains finite at low temperatures as can be seen in Fig. 2 of Ref. 3 even after subtracting the Curie term coming from the presence of impurities. This situation seems to suggest that the formation of nonmagnetic local spin-singlets occurs below the transition temperature but that there still remain interacting magnetic spins.³ The broad nonmagnetic spectrum in the insulating region observed in a recent NMR experiment¹⁴ might also be interesting in this respect.

We therefore argue that these experimental situations are of possible relevance with the spin structure shown in Fig. 8 (b) where the local spin-singlets of two $s = 1/2$ spins coexist with the antiferromagnetically interacting local high-spin clusters.

IV. SUMMARY

We have studied the electronic and magnetic properties in hollandite vanadate $\text{K}_2\text{V}_8\text{O}_{16}$, a possible charge and orbital ordering system with the mixed valent state of V ions with $3d^2 : 3d^1 = 1 : 3$ and with the t_{2g} orbitals of V ions aligned on the 1D zigzag chains. First, we have calculated the Madelung energy of the system and obtained the most stable CO pattern that is consistent with the superlattice structure observed in experiment. Then, by using the second-order perturbation theory starting from the triply-degenerate t_{2g} orbitals in the VO_6 octahedral structure, we have derived the effective spin-orbit Hamiltonian. Here, we have evaluated the effect of distortions of the VO_6 octahedra from the local symmetry of the Madelung site potential, which justifies the assumption that the electrons do not occupy the d_{xy} orbital. Within the approximation of neglecting the small off-diagonal hopping parameters, we have found that the Hamiltonian is block-diagonal with vanishing orbital off-diagonal sectors. We then have used the numerical exact-diagonalization technique on small clusters and have obtained the orbital-ordering pattern in the ground state. We have also calculate the spin-spin correlation functions and have found that, depending on the parameter values, either the state of the antiferromagnetically fluctuating local high-spin clusters or the state of the local spin-singlets of two $s = 1/2$ spins coexisting with the local high-spin clusters of $S = 3/2$ is realized. By comparing these results with available experimental data which are quite limited at present, we suggest that the latter state can be in agreement with the electronic ground state of hollandite vanadate $\text{K}_2\text{V}_8\text{O}_{16}$.

Because our study presented here contains series of theoretical predictions on the outcome of future experimental studies, we hope that the present study will help one understand the nature of the charge, orbital, and spin degrees of freedom of this intriguing material.

Acknowledgments

We would like to thank M. Isobe, M. Itoh, and K. Okai for useful discussions on the experimental aspects of $\text{K}_2\text{V}_8\text{O}_{16}$. This work was supported in part by Grants-in-Aid for Scientific Research (Nos. 18028008, 18043006, 18540338, and 19014004) from the Ministry of Education, Culture, Sports, Science and Technology of Japan. A part of computations was carried out at the Research Center for Computational Science, Okazaki Research Fa-

ilities, and the Institute for Solid State Physics, University of Tokyo.

-
- ¹ M. Isobe and Y. Ueda, *J. Phys. Soc. Jpn.* **65**, 1178 (1996).
² T. Ohama, H. Yasuoka, M. Isobe, and Y. Ueda, *Phys. Rev. B* **59**, 3299 (1999).
³ M. Isobe, S. Koishi, N. Kouno, J. Yamaura, T. Yamauchi, H. Ueda, H. Gotou, T. Yagi, and Y. Ueda, *J. Phys. Soc. Jpn.* **75**, 73801 (2006).
⁴ H. F. Pen, J. Brink, D. I. Khomskii, and G. A. Sawatzky, *Phys. Rev. Lett.* **78**, 1323 (1997).
⁵ H. F. Pen, L. H. Tjeng, E. Pellegrin, F. M. F. de Groot, G. A. Sawatzky, M. A. van Veenendaal, and C. T. Chen, *Phys. Rev. B* **55**, 15500 (1997).
⁶ T. Waki, H. Kato, M. Kato, and K. Yoshimura, *J. Phys. Soc. Jpn.* **73**, 275 (2004).
⁷ Y. Shibata and Y. Ohta, *J. Phys. Soc. Jpn.* **71**, 513 (2002).
⁸ See, e.g., J. M. Ziman, *Principles of the Theory of Solids*, 2nd ed. (Cambridge University Press, London, 1972), pp. 37-42.
⁹ J. Kondo, Y. Asai, and S. Nagai, *J. Phys. Soc. Jpn.* **57**, 4334 (1988).
¹⁰ Y. Ohta, T. Tohyama, and S. Maekawa, *Phys. Rev. B* **43**, 2968 (1991).
¹¹ T. Mori, *J. Phys. Soc. Jpn.* **72**, 1469 (2003).
¹² W. Abriel, F. Rau, and K. J. Range, *Mater. Res. Bull.* **14**, 1463 (1979).
¹³ S. Horiuchi, Master thesis, Chiba University, 2008.
¹⁴ K. Okai and M. Itoh, private communication.
¹⁵ S. Miyasaka, Y. Okimoto, and Y. Tokura, *J. Phys. Soc. Jpn.* **71**, 2086 (2002).